Global and Planetary Change 239 (2024) 104503

Contents lists available at ScienceDirect

Global and Planetary Change

journal homepage: www.elsevier.com/locate/gloplacha

Hydroclimate variability in the Tropical Andes recorded by $\delta^{18}O$ isotopes from a new network of *Polylepis tarapacana* tree-rings

Claudio Álvarez [a,b,*], Duncan A. Christie [a,b,c,*], Álvaro González-Reyes [a,d,e,f], Thomas T. Veblen [g], Gerhard Helle [h], Carlos LeQuesne [a], Milagros Rodriguez-Caton [i,k], Paul Szejner [j], Felipe Flores-Sáez [a,c], Tania Gipoulou-Zúñiga [a], Manuel Suazo-Álvarez [a,b,c], Tomás Muñoz-Salazar [a,o], Diego Aliste [a], Mariano S. Morales [k], Ariel Muñoz [c,l,m,n], Ricardo Villalba [k]

[a] *Laboratorio de Dendrocronología y Cambio Global, Instituto de Conservación Biodiversidad y Territorio, Universidad Austral de Chile, Valdivia, Chile*
[b] *Cape Horn International Center (CHIC), Puerto Williams, Chile*
[c] *Center for Climate and Resilience Research (CR)², Santiago, Chile*
[d] *Instituto de Ciencias de la Tierra, Facultad de Ciencias, Universidad Austral de Chile, Valdivia, Chile*
[e] *Centro de Humedales río Cruces CEHUM, Universidad Austral de Chile, Chile*
[f] *Centro de Investigación Dinámica de Ecosistemas Marinos de Altas Latitudes - IDEAL, Chile*
[g] *Department of Geography, University of Colorado Boulder, USA*
[h] *German Research Centre for Geosciences, Climate Dynamics and Landscape Evolution, Potsdam 14473, Germany*
[i] *Department of Plant Sciences, University of California Davis, Davis, CA, USA*
[j] *Bioeconomy and Environment Unit, Natural Resources Institute Finland, Helsinki, Finland*
[k] *Instituto Argentino de Nivología, Glaciología y Ciencias Ambientales, CONICET, Mendoza 5500, Argentina*
[l] *Laboratorio de Dendrocronología y Estudios Ambientales, Instituto de Geografía, Pontificia Universidad Católica de Valparaíso, Valparaíso, Chile*
[m] *Centro de Acción Climática, Pontificia Universidad Católica de Valparaíso, Valparaíso, Chile*
[n] *Fundación San Ignacio del Huinay, Hualaihué, Chile*
[o] *Escuela de Graduados, Facultad de Ciencias Agrarias y Alimentarias, Universidad Austral de Chile, Valdivia, Chile*

ARTICLE INFO

Editor: Dr. Jed O Kaplan

Keywords:
Tropical Andes
$\delta^{18}O$
Soil moisture
Vapor pressure deficit
Hydroclimate

ABSTRACT

Stable oxygen isotopes records ($\delta^{18}O$) in tree-rings are commonly used to assess the response of trees to environmental variability being a valuable tool for studying past climate at different temporal and spatial scales. This is particularly relevant in semi-arid regions like the southern Tropical Andes, where ongoing environmental changes coincide with a rapidly increasing demand for hydrological resources, presenting a challenge for ecosystem dynamics and water resource management. In this study, we aim to determine the main spatio-temporal variability of a new network of $\delta^{18}O$ *Polylepis tarapacana* chronologies during the last century, and their relationships with hydroclimate and tropical circulation at local to subcontinental scales throughout the Tropical Andes. For this purpose, we develop six $\delta^{18}O$ *P. tarapacana* tree-ring chronologies across a 450 km latitudinal moisture gradient in the southern Tropical Andes adjacent to the Atacama Desert, covering the period 1900–2007. Results show a clear latitudinal gradient in the $\delta^{18}O$ values across the network and significant relationships are observed with other $\delta^{18}O$ tree-ring chronologies in Tropical South America, demonstrating clear regional climate influences at a subcontinental scale. A principal component analysis of the $\delta^{18}O$ tree-ring chronologies demonstrate a strong regional environmental signal contained in the network, exhibiting a main temporal pattern (PC1 $\delta^{18}O$) that explains 63% of the total variance during the period 1900–2007. Comparisons between PC1 $\delta^{18}O$ and environmental variables showed significant negative relationships with precipitation and soil moisture, and positive relationships with temperature and vapor pressure deficit (VPD) during summer when the South American monsoon occurs. The main $\delta^{18}O$ tree-ring network signal clearly records tropical atmospheric and circulation patterns across South America. The easterly wind flux conditions from the Amazon basin favor lower $\delta^{18}O$ values, and the PC1 $\delta^{18}O$ exhibit significant positive correlations with VPD across the entire

* Corresponding authors at: Laboratorio de Dendrocronología y Cambio Global, Instituto de Conservación Biodiversidad y Territorio, Universidad Austral de Chile, Valdivia, Chile.
E-mail addresses: dendro.alvarez@gmail.com (C. Álvarez), duncanchristieb@gmail.com (D.A. Christie).

https://doi.org/10.1016/j.gloplacha.2024.104503
Received 29 January 2024; Received in revised form 17 May 2024; Accepted 26 June 2024
Available online 28 June 2024
0921-8181/© 2024 Elsevier B.V. All rights are reserved, including those for text and data mining, AI training, and similar technologies.

Tropical Andes and the northern portion of the Amazon basin, and as well as outgoing longwave radiation across the southern Tropical Andes and part of the Amazon basin. The close relationships between the regional signals from our $\delta^{18}O$ tree-ring network with the previously mentioned parameters, highlight the potential to develop future hydroclimatic-related reconstructions with these $\delta^{18}O$ records to assess climate variability and change across the Tropical Andes.

1. Introduction

The composition of stable oxygen isotopes in tree-ring cellulose is a valuable tool for studying past climate and environmental variability (Naulier et al., 2015; Rinne et al., 2013; Treydte et al., 2024). The annual and even seasonal resolution of tree rings, the preservation of the isotopic signal over time, and the relationships between stable isotopes and environmental parameters have allowed the monitoring and reconstruction of multiple parameters, significantly complementing those generated using tree ring widths (Gagen et al., 2010; Leavitt and Lone, 1991). Stable oxygen isotopes in plants, inferred through the measurement of the $^{18}O/^{16}O$ ratio and expressed as $\delta^{18}O$, provide crucial information about the gas exchange between the atmosphere and the leaf water of trees (Farquhar and Lloyd, 1993). It has been documented that $\delta^{18}O$ in tree rings is influenced by the temporal variability in the isotopic content of water sources used by the plants, the isotopic enrichment in leaf transpiration controlled by vapor pressure deficit (VPD), and the percentage of isotopic exchange of oxygen post-assimilation before and during cellulose synthesis (Roden et al., 2000; Szejner et al., 2020; Treydte et al., 2014). Isotopic fractionation occurs during the leaf transpiration through the stomata, resulting in a higher proportion of $\delta^{18}O$ in the leaf water. This is due to the preferential evaporation of lighter isotopes (^{16}O) over the heavier isotopes (^{18}O). As a result, the water remaining in the leaves becomes enriched in $\delta^{18}O$ compared to the water in the soil (Roden et al., 2000; Szejner et al., 2020). The $\delta^{18}O$ values in tree rings may be influenced by patterns in the $\delta^{18}O$ of the water source, which reflect the evaporation and condensation within air masses and the distance from ocean sources on various spatial and temporal scales (Dansgaard, 1964). Therefore, $\delta^{18}O$ in tree rings can be an extremely useful tool for monitoring local and large-scale climate and related environmental variables at different temporal and spatial scales.

Environmental parameters that can be recorded in $\delta^{18}O$ chronologies include the integration of variations in $\delta^{18}O$ of source water and the evaporative enrichment at the leaf level driven by the vapor pressure deficit (VPD). Soil moisture is a crucial environmental variable related with the isotopic content of soil water and is of interest due to its potential connection between the $\delta^{18}O$ value in precipitation (water source) and $\delta^{18}O$ in tree growth rings (Treydte et al., 2014; Xu et al., 2020). The $\delta^{18}O$ values recorded in tree rings are likely influenced by the evaporation of water from the soil, resulting in an enrichment of the isotopic composition of the available water that is eventually absorbed by the trees (Bailey et al., 2023). Due to the lack of in-situ soil moisture measurements in remote areas, the use of satellite-based measurements, climate reanalysis, and data assimilation is crucial for assessing this variable, but these methods only encompass the last four decades (Martens et al., 2017). Moreover, VPD represents the atmospheric evaporative demand and influences the leaf-level transpiration of plants and the corresponding stomatal conductance (Roden et al., 2000; Treydte et al., 2014). VPD is the difference between the amount of moisture in the air and the amount of moisture that the air can hold when it is saturated. When the VPD increases, the amount of moisture in the air relative to its saturation capacity is reduced, and the air becomes drier (Rawson et al., 1977). Consequently, during evapotranspiration in conditions of a dry atmosphere, VPD determines a more intense enrichment in $\delta^{18}O$ due to the preferential evaporation of the lighter isotope (Craig and Gordon, 1965; Roden et al., 2000).

Oxygen isotopes ($\delta^{18}O$) are recorded in various natural archives, including tree rings, ice cores, lake sediments, corals, and speleothems. Oxygen isotopes in tree rings have been utilized as proxies for reconstructing past climatic and environmental conditions (Freund et al., 2023; Meier et al., 2020; Nagavciuc et al., 2022, 2024; Rinne et al., 2013; Rodríguez-Catón et al., 2024, Treydte et al., 2024). These reconstructions offer valuable insights into past climate variability, allowing us to understand temporal climate changes in periods beyond available instrumental records. This approach is particularly useful in remote regions, such as the southwestern Altiplano, where climatic information is limited and scattered, and can register latitudinal hydroclimatic fluctuations related to changes in relative humidity (Rodríguez-Catón et al., 2024). For most of the year the southwestern Altiplano experiences extremely dry conditions, with the exception of the summer months (November to March) when more than 70% of the annual total precipitation occurs (Garreaud et al., 2003; Vera et al., 2006). This precipitation is related to convective storms associated with the South American Summer Monsoon system SASM (Garreaud et al., 2003; Vuille and Keimig, 2004). These seasonal rains occur due to instability in the local troposphere, caused by intense surface heating and the establishment of easterly winds at higher altitudes, facilitating the transport of moist air masses from the Amazon basin (Garreaud et al., 2003). The Bolivian High, an anticyclonic system located over Bolivia, is a crucial atmospheric feature associated with the SASM. The geographic location and intensity of the Bolivian High play a significant role in precipitation patterns by regulating circulation patterns in the upper troposphere (Garreaud and Aceituno, 2001; Vuille and Keimig, 2004). The wet (dry) periods are associated with a strengthening (weakening) and a pronounced shift southward (northward) of the Bolivian High. This movement facilitates the expansion, through the simple horizontal advection of zonal winds from the east (west) in the upper atmosphere and the input (blocking) of humidity over the Altiplano (Falvey and Garreaud, 2005). Consequently, the interplay between the dynamics of the Bolivian High and the easterly winds in the upper troposphere critically influences precipitation patterns over the Altiplano (Falvey and Garreaud, 2005; Garreaud and Aceituno, 2001; Garreaud et al., 2003; Vuille and Keimig, 2004). On the other hand, rainfall originating from the west is uncommon because the moisture from the Pacific is vertically captured due to the large-scale anticyclonic subsidence and highly stable low-level thermal inversion along the Pacific coast. Additionally, the Bolivian High blocks the atmospheric circulation from the west (Garreaud et al., 2003). Therefore, the study of the hydroclimate of the Altiplano not only sheds light on the behavior of the climate on a local scale but also on a regional scale across the Tropical Andes and the areas influenced by the South American monsoon. Understanding the variability of hydroclimate in the Altiplano is essential to assess the vulnerability of natural ecosystems and for effective water resource management for human activities. In recent decades, a concerning negative trend in precipitation has been observed, accompanied by extreme events such as droughts, which have caused severe impacts on ecosystems, as well as agricultural and livestock activities in the Altiplano region (Canedo-Rosso et al., 2021; Morales et al., 2020). This becomes even more concerning given that there are projections indicating an increase in the frequency of droughts in the Altiplano (Minvielle and Garreaud, 2011; Neukom et al., 2015). The analysis of oxygen isotopes in the Altiplano region thus becomes a fundamental tool for unraveling climatic patterns over time, providing a more comprehensive perspective on the climatic history of the region.

Polylepis tarapacana is the tree species that grows at the highest altitude in the world (up to 5200 m a.s.l.) within the Altiplano plateau at

the southern portion of the Tropical Andes (16°-22° S; Braun, 1997). Currently, this semiarid biome is highly threatened by anthropogenic activity (Messerli et al., 1997), the increase in air temperature (Vuille et al., 2015) and the projected decrease in precipitation (Minvielle and Garreaud, 2011; Neukom et al., 2015). These factors are projected to result in a severe reduction in the potential distribution of *P. tarapacana* by the end of the 21st century due to more arid conditions (Cuyckens et al., 2016). *P. tarapacana* woodlands provide numerous ecological services in the Tropical Andes, including specific habitats for bird and animal species, reduction of soil erosion, water provision, and source of wood and medicinal plants for local communities (Cuyckens et al., 2016). This species presents distinguishable annual growth rings and can live for more than 750 years, serving as an excellent environmental archive for the semiarid Tropical Andes. It has been useful for reconstructing regional hydroclimate using its ring widths (Morales et al., 2012, 2023). Several tree-ring studies show a significant positive relationship between previous growing season moisture conditions and *P. tarapacana* radial growth (Christie et al., 2009; Solíz et al., 2009; Morales et al., 2012, 2020). Recent studies assessing stable isotope in *P. tarapacana* tree rings have determined close relationships between $\delta^{13}C$ and $\delta^{18}O$ content with climate variables, indicating a significant negative (positive) relationship between $\delta^{18}O$ and precipitation (temperature) during the current growing season (Rodríguez-Catón et al., 2021). Additionally, Rodríguez-Catón et al. (2022) recorded a high temporal and spatial coherence between *P. tarapacana* $\delta^{18}O$ chronologies located in Chile and Bolivia, demonstrating the suitability of these records to develop climate reconstructions in the southern Altiplano. These results highlight the utility of *P. tarapacana* $\delta^{18}O$ chronologies to record past hydroclimate as recently demonstrated by Rodríguez-Catón et al. (2024). However, there is a need to develop future hydroclimate reconstructions in the region based on $\delta^{18}O$ tree-ring networks to increase the regional spatial coverage of these records and capture subcontinental signals throughout the Tropical Andes.

This research presents a new network of annual resolution *P. tarapacana* $\delta^{18}O$ chronologies. The network spans the period 1900–2007 and comprises six chronologies located along a 450 km latitudinal moisture gradient in the southern Tropical Andes, adjacent to the Atacama Desert. This network is employed to (i) characterize the $\delta^{18}O$ variability of tree-ring sites along the gradient, (ii) determine the main spatio-temporal pattern of variability in $\delta^{18}O$ records during the 1900–2007 period, and (iii) assess the relationships between the main pattern of $\delta^{18}O$ variability across the network with climate and environmental variables at local to subcontinental scales throughout the Tropical Andes.

2. Methods

2.1. Study area

The collection of *P. tarapacana* samples were conducted between 2008 and 2017 in the southwestern region of the semiarid Tropical Andes in the Altiplano region, sampling six sites along a latitudinal gradient of aridity extending approximately 450 km between 17°S and 21°S in Chile along the border with Bolivia (Fig. 1, Table 1). The sites are located at an average altitude of 4500 m a.s.l. on moderate slopes with soils of volcanic origin. The Altiplano is a high-elevation semi-arid

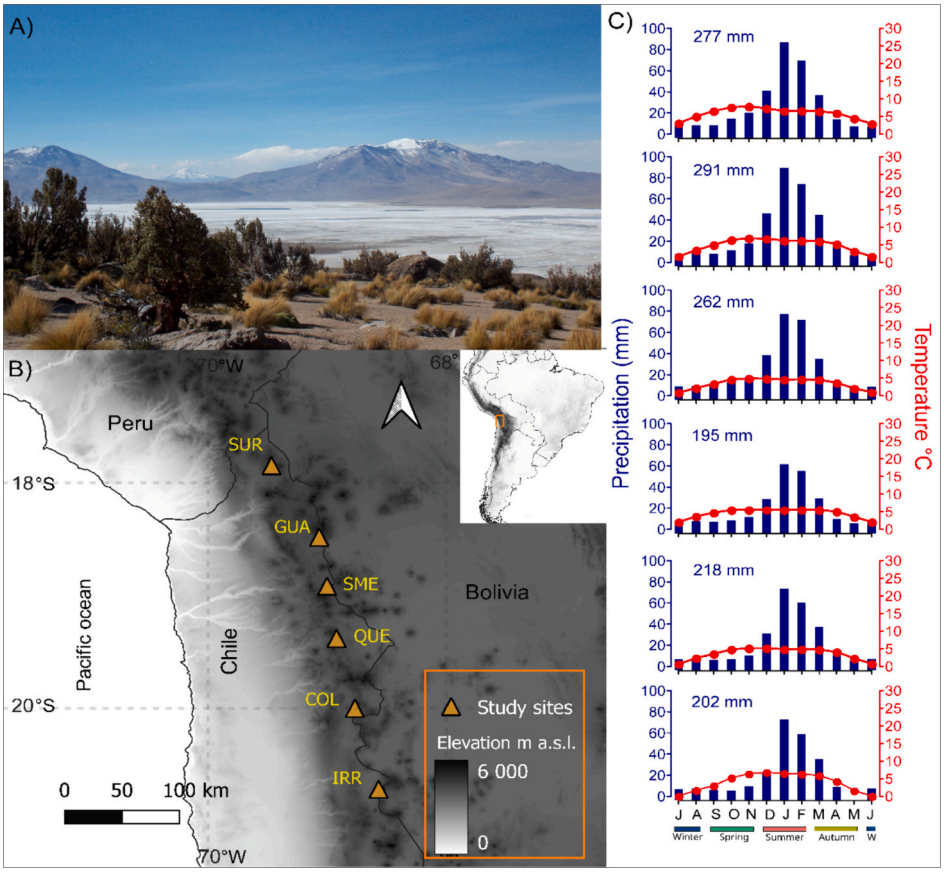

Fig. 1. (a) *Polylepis tarapacana* woodlands in the Surire Medio site (SME) at 4650 m a.s.l. in Chile. At the back the Salar de Surire salt lake and the Arintica and Puquintica volcanoes, the last one, border with Bolivia. (b) Location of the six sites analyzed across the latitudinal gradient in the southern Tropical Andes in Chile (orange triangles): Suriplaza (SUR), Guallatire (GUA), Surire (SME), Queñiza (QUE), Collacagua (COL) and Irruputuncu (IRR). (c) Annual cycle of mean monthly temperature (red line) from CRU dataset and mean monthly precipitation at each study site (blue bars) from CR2MET dataset gridded product during the period 1981–2020. (For interpretation of the references to colour in this figure legend, the reader is referred to the web version of this article.)

Table 1
Characteristics of the tree-ring width and $\delta^{18}O$ *Polylepis tarapacana* chronologies.

Sites	SUR	GUA	SME	QUE	COL	IRR
Lat & Lon	17.9°S 69.5°W	18.5°S 69.1°W	18.9°S 69.0°W	19.4°S 68.9°W	20.0°S 68.8°W	20.7°S 68.6°W
Altitude (m a.s.l.)	4760	4570	4640	4380	4200	4320
Number of series	48	129	47	56	83	110
Series inter-correlation	0.56	0.63	0.62	0.63	0.60	0.58
Mean TRW (mm) +/− SD	0.66 +/− 0.4	0.43 +/− 0.2	0.52 +/− 0.2	0.51 +/− 0.3	0.50 +/− 0.3	0.52 +/− 0.3
Mean sensitivity	0.35	0.28	0.29	0.31	0.39	0.33
Rbar (mean)	0.29	0.32	0.38	0.42	0.40	0.35
Missing ring (%)	0	0.004	0	0.050	0.013	0.014
EPS > 0.85	1770–2007	1395–2015	1490–2009	1550–2007	1400–2015	1430–2015
SNR	17.25	85.37	64.67	57.73	26.87	17.54
Autocorrelation	0.41	0.57	0.51	0.59	0.58	0.71
Mean chron $\delta^{18}O$ (‰) +/− SD (1900–2007)	29.0 +/− 1.5	30.1 +/− 1.7	30.4 +/− 1.4	31.1 +/− 1.2	32.7 +/− 1.3	32.9 +/− 1.4

SUR = Suriplaza, GUA = Guallatire, SME = Surire medio, QUE = Queñiza, COL = Collacagua and IRR = Irruputuncu. SD = standard deviation, TRW = Tree-ring width, EPS = Expressed population signal. Rbar is the mean correlation coefficient for all possible pairings among tree-ring series from individual cores, computed for a specific common time interval. To compute EPS and Rbar parameters we used a 50-year window with a 25-year overlap (Briffa 1995). SNR = Signal-to-noise ratio. SNR was calculated following the methodology of Cook and Pederson (2011) and using dplR package in R (Bunn, 2008).

mountain plateau with a mean elevation of 4000 m a.s.l. and situated between 15°S and 23°S in the southern Tropical Andes. The summits in this area generally reach altitudes of 6000 m a.s.l. The Tropical Andes at the Altiplano act as a barrier to tropospheric circulation, creating two contrasting climatic regions. One region is located to the east on the tropical lowlands with high humidity and precipitation, while the other is located to the west, toward the Pacific coast in the Atacama Desert (Garreaud et al., 2003). The study sites are located across a moisture gradient in the southern portion of the Tropical Andes, where the climate is characterized as semiarid to arid. The site furthest north (SUR) received 277 mm of precipitation per year, while the site furthest south received 202 mm of precipitation per year (IRR; Fig. 1c). For each study site, a monthly cycle of precipitation was developed using gridded data from CR2MET (Boisier, 2023) available at https://www.cr2.cl/datos-productos-grillados/ (Fig. 1c). These data have a spatial resolution of 0.05° x 0.05° and cover the period 1979–2020. The CR2MET precipitation field is based on statistical models that translate precipitation data from ERA-Interim (Dee et al., 2011) into better regional estimates for Chile by incorporating topography and by calibrating with local meteorological stations, and it has proven to be an excellent dataset for the Altiplano region (Anderson et al., 2021). For temperature, we used the CRU gridded dataset with a resolution of 0.5° x 0.5° (Harris et al., 2020).

2.2. Development of chronologies and preparation of samples for isotopes analysis

P. tarapacana is a small evergreen angiosperm that can reach a height of 2–3 m and grows along the Altiplano in the southern Tropical Andes between 16°S and 22°S, at altitudes ranging from 4000 to 5200 m (Christie et al., 2009; Morales et al., 2012). It grows in semi-arid conditions with high solar radiation and experiences wide daily temperature ranges, with differences of up to 16 °C between day and night (García-Plazaola et al., 2015). The sampling strategy targeted adult trees from woodland patches without evidence of human disturbance such as logging and/or fire located at the mid elevation of the species local altitudinal distribution. Given the eccentric growth pattern of the species, we collected cross sections from one of the multiple stems of trees and subfossil material. The number of trees per site are indicated in Table 1. Samples were prepared using standard dendrochronological techniques (Stokes and Smiley, 1968). The samples were dated using the Schulman (1956) convention for the Southern Hemisphere, which assigns to each annual ring the date of the calendar year in which tree growth began. Ring widths were measured with an accuracy of 0.001 mm under a microscope with a Velmex measuring station (Velmex Inc., Bloomfield NY, USA) connected to a computer. To identify potential dating errors due to partially missing rings, false rings, or incorrect measurements, the COFECHA software was used (Holmes, 1983). Each series was detrended using a negative exponential curve or a straight line using the ARSTAN software (Cook et al., 1990). This procedure removes the effects of age and potential disturbances in ring widths (Fritts, 1976), transforming the series to values of a dimensionless index. The expressed population signal (EPS) and Rbar were used to assess the quality of the chronologies. EPS estimates the closeness of a finite-replicated chronology to a hypothetical perfect chronology based on infinite trees (Wigley et al., 1984). Rbar is the mean correlation coefficient of all possible pairings among tree-ring series from individual cores, computed for a specific common time interval (Briffa, 1995). To calculate the EPS and Rbar, we used a 50-year window with a 25-year overlap between adjacent windows.

After each sample was correctly dated, a tree-ring width chronology was generated at each site. From each ring-width chronology, five trees were selected for isotope analysis based on the following criteria: tree-ring samples with distinct and well-defined wide rings, trees older than 150 years to avoid potential age-related effects, and series showing significant correlations with the site-level ring-width chronology. Using a microscope, each growth ring from the five selected trees was carefully cut with a scalpel and combined to create a composite sample for each year spanning the period 1900–2007. As a result, six combined $\delta^{18}O$ stable isotope chronologies of *P. tarapacana* were developed, one for each site covering the period 1900–2007. In addition, to assess the annual variability of $\delta^{18}O$ among the individual trees contributing to the composite chronologies at each sampling site, samples were collected in each year of a new decade (i.e. 11 years between 1900 and 2000). For this set of samples, the $\delta^{18}O$ content was determined individually for each of the five trees at each site. Previous studies of $\delta^{18}O$ content in *P. tarapacana* have shown extremely high coherence between $\delta^{18}O$ individual series, demonstrating a high coherence in the interannual variability of tree-ring $\delta^{18}O$ values from different trees using five trees (Rodríguez-Catón et al., 2021).

In total, the isotopic ratios of oxygen ($^{18}O/^{16}O$) of 967 tree-ring cellulose samples were determined, with 648 determinations for the six composite chronologies and 319 determinations for the individual tree samples. The $^{18}O/^{16}O$ ratios were expressed in the conventional d-notation:

$$\delta‰ = [(\text{Rsample} - \text{Rstandard})/\text{Rstandard})]^{*} 1000$$

where R represents the ratio ($^{18}O/^{16}O$) between heavier (^{18}O) and lighter (^{16}O) oxygen isotope species, specifically related to the Vienna Standard Mean Ocean Water (VSMOW) for $\delta^{18}O$.

Isotope analyses were conducted at the Tree-Ring Laboratory at German Research Centre for Geosciences GFZ in Potsdam, Germany. Holocellulose was extracted from whole wood using the two-step base-acid method: sodium hydroxide for resin and extractives removal

followed by acidified sodium chlorite to eliminate lignins (Helle et al., 2022). Following extraction, samples were washed thoroughly with milli-Q water, homogenized (ultrasonic sonode device for Eppendorf sample vials) and then freeze-dried for 48 h (Laumer et al., 2009). Resultant homogenized cellulose was weighed (160-200 μg) and packed in silver capsules for stable oxygen isotope analysis. Measurements were completed on an Isotope Ratio Mass Spectrometer Delta V, Thermo-Fisher Scientific, Bremen, Germany with TC/EA HT pyrolysis device at 1400 °C. The samples analyzed are referenced to standard materials from the International Atomic Energy Agency (IAEA-C3, IAEA-CH6, IAEA-601 and IAEA-602), and checked with secondary standards from Sigma-Aldrich Chemie GmbH, Munich, Germany (Sigma Alpha-Cellulose and Sigma Sucrose) using a two-point normalization method (Paul et al., 2007). Sample replication resulted in a reproducibility of better than ±0.3‰ for the $\delta^{18}O$ values.

2.3. Climate data

In order to assess the relationships between $\delta^{18}O$ tree-ring chronologies and local climate, we utilized the regional datasets of precipitation and temperature developed by Rodríguez-Catón et al. (2021). These datasets were constructed using data from 36 weather stations located in the Andes of Chile, Bolivia, Argentina, and Peru. The regional mean precipitation covered the period from 1950 to 2008, while the temperature series covered the period from 1951 to 2008, respectively. The decision to use climate data from weather stations starting from 1950 were based on the availability and reliability of the data in the remote Andean region of the study area. We used soil moisture data from the grid points of tree-ring sample sites, which were obtained from the Famine Early Warning Systems Network Land Data Assimilation System (FLDAS; McNally et al., 2017). This global land surface model is driven by various datasets from satellite measurements and atmospheric analyses, which are evaluated using direct comparisons of outputs with independent measurements (ground/satellite) and indirect comparisons, including correlations of soil moisture with vegetation indices (McNally et al., 2017). The FDLAS data provides monthly gridded soil moisture data at various depths, with a horizontal resolution of approximately 10 km since the year 1982. The data is expressed as the volume of water per soil volume (m^3/m^3). For our research, we focused on the soil moisture layer between 0 and 10 cm and 10–40 cm in depth. We used gridded (0.5° x 0.5°) mean monthly temperature and relative humidity data obtained from the Climate Research Unit (CRU) (Harris et al., 2020) to calculate VPD. First, we calculated saturation vapor pressure e_s in millibars using the equation developed by Hartmann (2016).

$$e_s = 6.11^{*}exp\left(\frac{L}{Rv}\left(\frac{1}{273}-\frac{1}{T}\right)\right)$$

where L represents the latent heat of evaporation (2.5×10^6 J Kg^{-1}), Rv is the gas constant for water vapor (461 J K^{-1} Kg^{-1}), and T is the temperature in degrees Kelvin. Based on the e_s, VPD was calculated using the equation:

$$vpd = \frac{e_s^{*}(100 - RH)}{100}$$

where RH represents the relative humidity in percentage. Precipitation and temperature gridded data from 0.25° x 0.25° ERA5 reanalysis (Hersbach et al., 2020) were utilized for field correlation maps. Outgoing longwave radiation (OLR) and zonal and meridional wind data were obtained from 0.25° x 0.25° ERA5. In Tropical South America, negative (positive) OLR are indicative of enhanced (suppressed) convection and hence more (less) cloud coverage and precipitation, representing a common method to study these hydroclimatic parameters in the region (Liebmann and Smith, 1996; Vuille and Keimig, 2004).

2.4. Geographical provenance of air parcels

We used the HYSPLIT (Hybrid Single-Particle Lagrangian Integrated Trajectory) model to assess the potential geographical provenance of the air parcels that transported humidity to each tree-ring sampling site across the north-south latitudinal gradient of the network. HYSPLIT is an atmospheric transport and dispersion model designed to calculate simple air-parcel trajectories and the movement of particles through the atmosphere (Draxler and Hess, 1998; Stein et al., 2015). Following Ancapichún et al. (2021), we calculated one trajectory per day for each tree-ring site, starting at 15:00-UTC and extending 240 h backward during the *P. tarapacana* summer growing season (December through March). Each backward trajectory represents the spatial displacement of air parcels over a 10-day period (240 h). The total study period encompassed 58 years, starting in 1950 and ending in 2008. This approach resulted in 6975 trajectories for each tree-ring site, completing 41,850 trajectories across the latitudinal gradient of the tree-ring network. Following Stein et al. (2015) and Ancapichún et al. (2021), and evaluating the topography of the region, we used 550 hPa (~5000 m) as the starting point of the air parcel analysis to ensure the reliable performance of the HYSPLIT model. The NCEP/NCAR reanalysis was used as the input data of the HYSPLIT model (Kalnay et al., 1996), and finally, the calculated backward trajectories were generated as a set of longitudinal, latitudinal, and altitudinal points based on 240 h into the past for a specific hour of the day (Draxler and Taylor, 1982), in our case 15:00 UTC.

Two analytical approaches were applied for each tree-ring site leveraging the output of the HYSPLIT model: (i) to assess the frequency location of the total number of air parcel of all backward trajectories passing through each geographical grid, and (ii) to calculate the average value of the relative humidity from all trajectories passing through each geographical grid. The HYSPLIT model calculation was performed in R using the openair package (Carslaw and Ropkins, 2012), and the maps were developed with the m_map package in Matlab software (Pawlowicz, 2020).

2.5. Spatio-temporal patterns of $\delta^{18}O$ variability and climate relations

A Principal Component Analysis (PCA) was conducted to identify the common regional signal among the six $\delta^{18}O$ chronologies of *P. tarapacana* over the 1900–2007 period. The loadings of each $\delta^{18}O$ chronology with the main mode of $\delta^{18}O$ variability (PC1) were calculated as the correlation coefficient between each $\delta^{18}O$ chronology and the PC1 time-series over the period 1900–2007, and the results were plotted on a map.

To identify the relationships between climatic and environmental factors and $\delta^{18}O$ variability, correlation functions were computed between the time series of the first two modes of $\delta^{18}O$ variability (PC1 $\delta^{18}O$ and PC2 $\delta^{18}O$) and soil moisture (at 0–10 cm and 10–40 cm), as well as the regional series of precipitation and temperature (Blasing et al., 1984). The correlation analyses were conducted using the treeclim package (Zang and Biondi, 2015), available in the free statistical software R (R Development Core Team, 2021). To determine the relationships between the main mode of $\delta^{18}O$ *P. tarapacana* variability (PC1 $\delta^{18}O$) and atmospheric and climatic features, correlation maps were calculated between PC1 $\delta^{18}O$ and the summer (DJFM) averaged 0.25° × 0.25° gridded OLR from ERA5, serving as a measure of convection, as well as 0.5° × 0.5° gridded VPD derived from CRU. Additionally, to assess atmospheric circulation patterns associated with convection and the South American monsoon activity, following Christie et al. (2011) the 10 highest and 10 lowest PC1 $\delta^{18}O$ values (years) within the period 1950–2008 were selected as indicators of the 10 driest and 10 wettest years, respectively. Using these values, the mean summer (DJFM) circulation patterns related to the 200 hPa zonal and meridional wind components anomalies were calculated, covering the reference period from 1950 to 2007. This enables the creation of two separate composite

200 hPa wind anomaly fields, and the difference between them (dry minus wet years as inferred from the PC1 $\delta^{18}O$ series) Plotted. The correlations and composite maps were generated using the m_map package in Matlab software (Pawlowicz, 2020). All correlations were assessed after removing the red noise from the time series by pre-whitening using an autoregressive (AR) model, where the order was estimated by means of AIC (Akaike, 1974). This step prevents the adjustment of degrees-of-freedom for the serial persistence seen in the original data to properly test correlation significance (e.g., Dawdy and Matalas, 1964).

3. Results

3.1. Oxygen stable isotope chronologies

Six $\delta^{18}O$ chronologies were developed from *P. tarapacana* tree-ring cellulose, covering the period from 1900 to 2007 across a 450 km latitudinal moisture gradient in the Southern Tropical Andes (Fig. 2). A high similarity between the $\delta^{18}O$ chronologies at interannual variability was recorded along the environmental gradient. The $\delta^{18}O$ analysis at annual resolution in each year of a new decade from individual trees per site (11 years between 1900 and 2000) exhibited high similarity among the $\delta^{18}O$ values at each site (Fig. S1). In general, the $\delta^{18}O$ chronologies showed a decrease of 5% around 1910 with respect to the mean, followed by a subsequent recovery of 5% around 1913. Then, $\delta^{18}O$ chronologies showed values around the mean up to the early 1960s, with a subsequent increase in their values of 9% in 1965 with respect to the mean. A decrease of 7% in $\delta^{18}O$ was observed in the early 1970s, followed by an increase of 5% in the early 1980s, another decrease of 6% in the mid-1980s, and finally an increase up to around the mean in the early 1990s. From the mid-1990s to 2007 the SUR, GUA, SME and QUE chronologies exhibited consistent and stable values among each other, remaining around its respective means. In contrast, the COL and IRR chronologies showed a slight increase in this period (Fig. 2a).

The PCA results from the six $\delta^{18}O$ *P. tarapacana* chronologies shows that the first mode of $\delta^{18}O$ variability (PC1) explain a large portion of the common variance (63%), where all chronologies have relatively similar loadings, demonstrating a strong regional environmental signal across the 450 km latitudinal moisture gradient (Fig. 2b, c). The loadings of each of $\delta^{18}O$ chronology with PC1 $\delta^{18}O$ (represented as the correlation coefficient between each $\delta^{18}O$ chronology and the PC1 over the 1900–2007 period) are SUR: 0.81, GUA: 0.84, SME: 0.87, QUE: 0.85, COL: 0.63, IRR: 0.76 (all significant at $p < 0.001$), with the southern sites exhibiting the lowest values (Fig. 2b). The second mode of $\delta^{18}O$ variability (PC2) explain a small portion of the common variance (12.9%), with loadings of SUR: -0.32***, GUA: -0.23**, SME: −0.13 ns, QUE: −0.07 ns, COL: 0.70***, IRR: 0.28* (*$p < 0.05$; **$p < 0.01$; ***p < 0.001; ns: not significant), demonstrating that PC2 represents a local signal related to the southern sites mainly by COL.

Moreover, a clear north-south gradient is observed in the distribution of the annual $\delta^{18}O$ values from the cellulose of each *P. tarapacana* chronology ($n = 108$; period 1900–2007) across the latitudinal moisture gradient (Fig. 3). The tree-ring sites toward the northern distribution exhibit lower $\delta^{18}O$ isotopic values, with a median of 28.93‰ for the northernmost site (SUR) and a median of 33.04‰ for the southernmost site (IRR) (Fig. 3). This pattern is also observed in the mean values of the $\delta^{18}O$ determinations for each year of a new decade from individual trees at each site (Fig. S1).

3.2. Humidity sources and geographical provenance of air parcels air

We used the HYSPLIT model to assess the potential geographical provenance of air parcels that transported humidity to each tree-ring sampling site across the north-south latitudinal gradient of the network. The six maps generated through the HYSPLIT backward trajectory analysis illustrate the frequency location and relative humidity

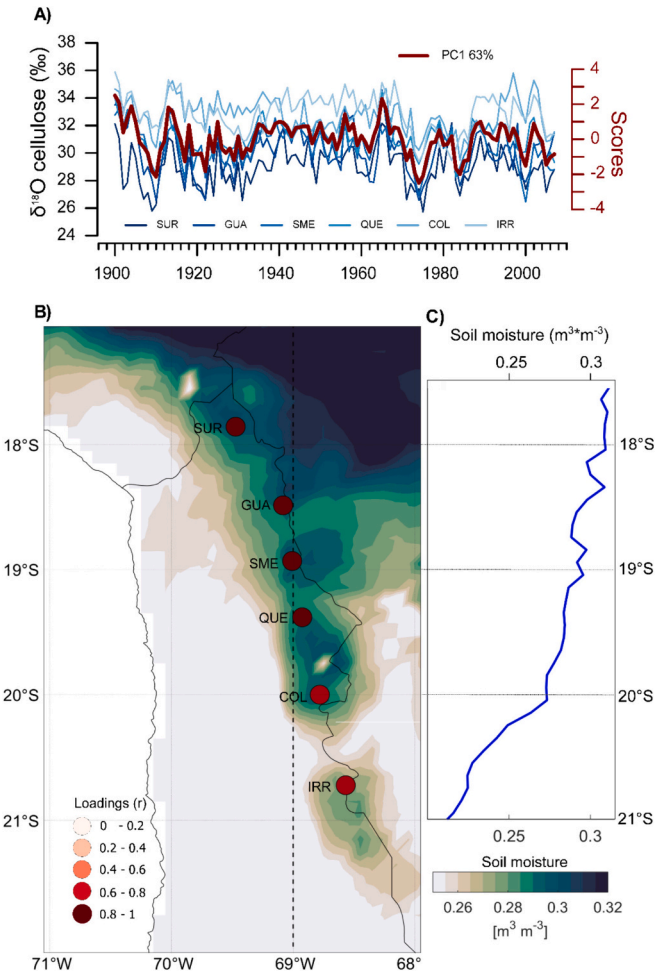

Fig. 2. Spatio-temporal patterns of $\delta^{18}O$ chronologies of *Polylepis tarapacana* across the 450 km latitudinal moisture gradient in the southern Tropical Andes. (a) The tree-ring cellulose $\delta^{18}O$ chronologies of *P. tarapacana* at each study site (intensity of blue corresponds to its latitudinal position), and the first Principal Component calculated from them (PC1 $\delta^{18}O$, red line) which explains 63% of the total variance for the period 1900–2007. (b) Location of $\delta^{18}O$ chronologies of *P. tarapacana* (circles) with colors indicating their loadings with respect to PC1 $\delta^{18}O$ expressed as the correlation coefficient between each $\delta^{18}O$ chronology and the PC1 for the period 1900–2007 (all correlations are significant at $p < 0.001$). Colour contours indicate the summer mean soil moisture ($m^3 * m^{-3}$) at a depth of 0–10 cm (December through March) covering the period 1982–2022 with a spatial resolution of 0.1° x 0.1°, obtained from the FLDAS Land Data Assimilation System dataset. (c) Corresponding summer soil moisture latitudinal gradient in the study area along the 69° W meridian (black dashed line in (b). (For interpretation of the references to colour in this figure legend, the reader is referred to the web version of this article.)

provenance of air parcels that transported humidity across the north-south moisture gradient of the network (Fig. 4). Each map delineates the potential geographical provenance of air parcels, with isolines indicating the frequency of air parcels passing through each geographical grid. The isolines help visualize areas with different numbers of air parcels, such as those with 600, 1000, 3000, and 30,000 air parcel locations. Additionally, the colorbar scale provides information on the average relative humidity from all trajectories passing through each geographical grid. (Fig. 4). Air parcels with higher percentages of relative humidity are observed over the Amazon basin and the opposite over the Pacific Ocean. The results indicate that concomitant with the north-south gradient of the tree-ring sites location, the number of wet parcels from the Amazon basin decreases while that of dry parcels from the Pacific increases. This is consistent with the soil moisture gradient of

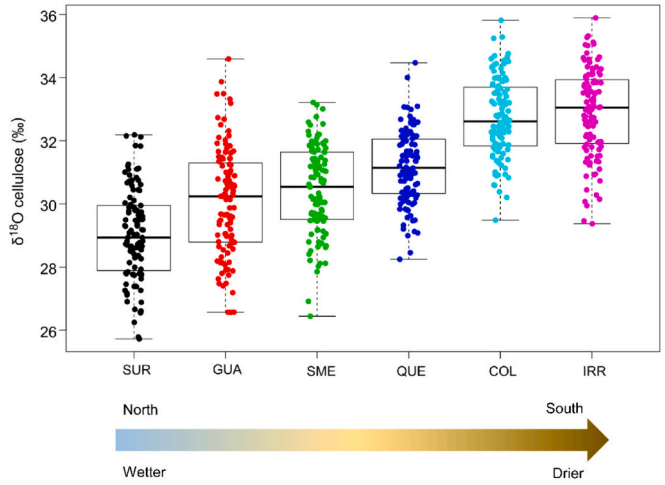

Fig. 3. Box-and-whisker plots exhibiting the distribution of all the 108 annual $\delta^{18}O$ values from the cellulose of *Polylepis tarapacana* chronologies of each sampling site across the latitudinal moisture gradient during the period 1900–2007 (north-south from left to right in the horizontal axis). The horizontal line inside each box represents the median, and the whiskers and the box limit the minimum, maximum values and the 25th and 75th percentiles, respectively. The tree-ring sampling sites are ordered in the horizontal axis from left to right according to its location across the north-south moisture gradient.

tree-ring sites shown in Fig. 2. Sites located further south across the latitudinal gradient (COL and IRR) exhibit a lower number of wet parcels from the Amazon basin and a higher number from the Pacific (Fig. 4).

3.3. Relationships between oxygen isotopes and climatic and environmental variables

During the Southern Hemisphere summer months, which are the rainiest months and the *P. tarapacana* growing season in the Altiplano, there is a significant negative correlation between precipitation and PC1 $\delta^{18}O$ (DJF; $r = -0.76$; $p < 0.01$; Fig. 5). The PC1 $\delta^{18}O$ also showed significant negative correlations with soil moisture (SM) at depth of 0–10 cm and 10–40 cm during the summer (JFM) months ($r = -0.76$ and $r = -0.67$, respectively, $p < 0.01$, Fig. 5b), with a remarkable interannual similarity, especially with SM at 0–10 cm (Fig. 5b). On the contrary, the PC1 $\delta^{18}O$ and mean temperature showed significant positive relationships during the summer (DJF; $r = 0.65$, $p < 0.01$, Fig. 5b). PC2 $\delta^{18}O$ showed no correlations with temperature and SM (10–40 cm), and only weak correlations with February precipitation from the previous year of ring formation and SM (0–10 cm) in October from the current season (Fig. S2).

The PC1 $\delta^{18}O$ shows negative correlations with precipitation over the southern Tropical Andes and part of the Amazon basin and positive with temperature across the entire Tropical Andes and the Amazon basin during the summer *P. tarapacana* growing season (DJFM) (Fig. 6). Correlation maps between PC1 $\delta^{18}O$ and OLR and VPD exhibit positive spatial relationships during summer (DJFM) (Fig. 7), being consistent with the spatial patterns of the relations between PC1 $\delta^{18}O$ and precipitation and temperature. With respect to OLR, the significant correlations are centered across the southern Tropical Andes, highlighting strong convective activity in the region (Fig. 7a). This pattern is consistent with the easterly air mass flux indicated by the wind vectors (Fig. 7a). The wind composite anomalies, derived from the difference between the composite maps of the 10 highest and 10 lowest PC1 $\delta^{18}O$ years (as indicators of the 10 driest and 10 wettest years, respectively), depict the classical spatial patterns of a strong convection and activity in the South American monsoon system (Fig. 7a) (Garreaud, 1999; Vuille and Keimig, 2004;). It is remarkable the results of the field correlation between PC1 $\delta^{18}O$ and VPD, which exhibit significant positive correlations across the entire Tropical Andes and the northern portion of the Amazon basin (Fig. 7b). This pattern is spatially consistent with the field correlations between gridded VPD and the regional time series of precipitation (negative) and temperature (positive) from the Altiplano during the summer (Fig. S3). Moreover, correlation maps between PC1 $\delta^{18}O$ and gridded precipitation and temperature during summer exhibit a consistent pattern with correlation maps between PC1 $\delta^{18}O$ and OLR and VPD (Fig. 7), with negative correlations over the southern Tropical Andes and part of the Amazon basin for precipitation and positive all across the Tropical Andes and the Amazon basin for temperature (Fig. 6).

4. Discussion

4.1. Spatiotemporal patterns of $\delta^{18}O$ chronologies

Six annually-resolved $\delta^{18}O$ chronologies from *P. tarapacana* in the Altiplano region reveal highly coherent spatiotemporal patterns of environmental variability in the southern Tropical Andes during the past century. The presented $\delta^{18}O$ *P. tarapacana* chronologies highlight a strong common signal between chronologies across a latitudinal gradient of 450 km across the region demonstrating similar climate and environmental variations registered in the records, highlighting their utility to describe regional past climate and environmental variability in the southern Tropical Andes. Despite the high loadings of all chronologies to the main mode of $\delta^{18}O$ variability, the southern sites exhibited slightly lower values, demonstrating some differences across the latitudinal moisture gradient (Fig. 2b). Interestingly, significant relationships of this new $\delta^{18}O$ *P. tarapacana* network are observed with other $\delta^{18}O$ tree-ring chronologies from Tropical South America. This includes the $\delta^{18}O$ *P. tarapacana* chronologies from Rodríguez-Catón et al. (2021) in the southern tropical Bolivian Andes, and the $\delta^{18}O$ *Cedrela* chronologies from Brienen et al. (2012); Baker et al. (2015, 2022) located about ~1000 km away from our network in the tropical lowlands of northern Bolivia (*C. odorata*) and > 2000 km away in the Ecuadorian Andes (*C. montana*) (Fig. 7b). The presented $\delta^{18}O$ P. tarapacana chronologies highlight a strong common signal among chronologies across a latitudinal gradient of 450 km across the region, demonstrating similar climate and environmental variations registered in the records, highlighting their utility to describe past climate and environmental variability at a subcontinental scale in the southern Tropical Andes.

The $\delta^{18}O$ *P. tarapacana* chronologies reveal a clear north-south isotopic gradient across the network, with an increase in mean $\delta^{18}O$ values toward the southern sites (Fig. 3). This result is consistent with the increasing aridity toward the southern region (Fig. 2b, c). These conditions may favor the enrichment of $\delta^{18}O$ in the soil and leaf water of *P. tarapacana* due to the evaporation of the lighter isotope ^{16}O (Hsieh et al., 1998; Barbour et al., 2004). While this finding is consistent with more severe aridity toward the southern tree-ring sites, it does not match the distillation theory (Dansgaard, 1964), which suggest that more enriched $\delta^{18}O$ values would be expected in the cellulose of trees located closer to the origin of the water source, in this case, the Amazon basin (Garreaud et al., 2003). This apparent contradiction can be explained by a local amount effect, where higher levels of precipitation lead to depletion in the soil-water $\delta^{18}O$ value because the ^{18}O molecule precipitates faster (Hsieh et al., 1998; Risi et al., 2008). Higher precipitation levels in the tree-ring sites toward the north, closer to the Amazon basin, lead to a depletion in the $\delta^{18}O$ of precipitation. This depletion may contribute to lower $\delta^{18}O$ values in *P. tarapacana* tree-ring cellulose at sites with a higher amount of precipitation. Additionally, the reduced precipitation values and lower cloud cover toward the south (Vuille and Keimig, 2004) may result in higher solar radiation and thus increased evapotranspiration (Rodríguez-Catón et al., 2021). Consequently, there would be an enrichment in $\delta^{18}O$ of the soil water and plant leafs,

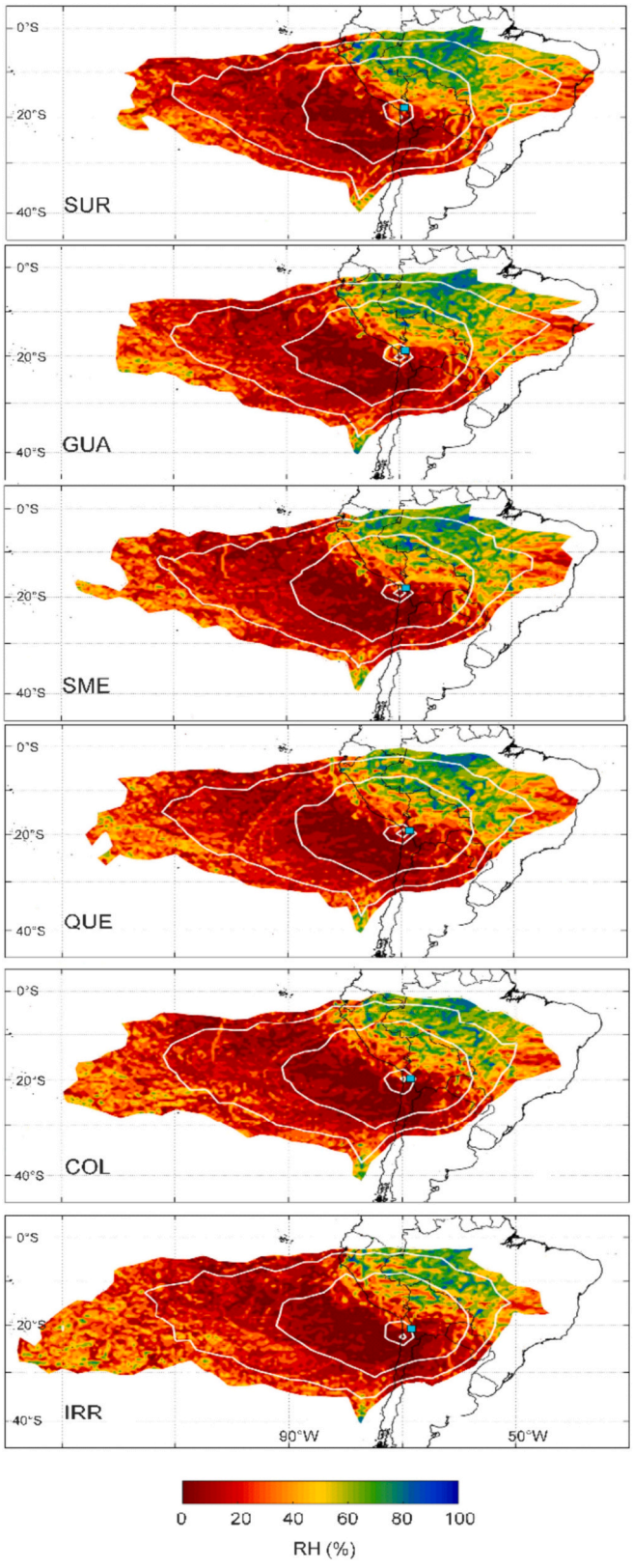

(caption on next column)

Fig. 4. HYSPLIT backward trajectory analysis of air parcels for each location of the *Polylepis tarapacana* tree-ring sites across the north-south (up-down) latitudinal gradient, using one trajectory per day, starting at 15:00-UTC and extending 240 h backward during summer (December through March) and covering the period 1950–2008 (6975 trajectories per site and 41,850 across the latitudinal gradient of the tree-ring network). In each panel the frequency of the total number of air parcels of all trajectories passing through each geographical grid are indicated by the five white isolines delimiting intervals of 600, 1000, 3000, 30,000 and 60,000 air parcels (from outer to inner, respectively), and the colorbar scale indicates the average value of the relative humidity (RH %) from all trajectories passing through each geographical grid (0.5° x 0.5°). Note that concomitant with the north-south gradient of the tree-ring sites location, the number of wet parcels from the Amazon basin decreases while that of dry parcels from the Pacific increase. In the lower left corner of each panel is indicated the code respective tree-ring site and the cyan rectangle its location on the map. (For interpretation of the references to colour in this figure legend, the reader is referred to the web version of this article.)

attributed to this increased aridity toward the southern portion of our latitudinal gradient.

4.2. Climate, atmospheric circulation and $\delta^{18}O$ chronologies relationships

The HYSPLIT results showed that the number of wet air parcels from the Amazon basin decreases across the north-south moisture gradient of the tree-ring network, while that of drier parcels from the Pacific increase (Fig. 4). This pattern may also contribute to the increasing north-south $\delta^{18}O$ gradient. Another potential factor contributing to the increasing north-south $\delta^{18}O$ *P. tarapacana* gradient is the larger influence of humidity source from the Pacific toward the southern sites. The noticeable decrease in the number of relatively more humid air parcels originating from the Amazon Basin toward the southern sites is concomitant with an increase of Pacific air parcels. Furthermore, toward the southern sites, there is an increase in humidity from the Pacific Ocean off the coast of Chile and subtropical latitudes, indicating the potential transport of air parcels with a higher percentage of relative humidity from higher latitudes (Fig. 4) (Vuille et al., 2003). The influence of air parcels and humidity sources varies with latitude, being more prominent from the Amazon Basin in northern sites (SUR and GUA), and with a more significant contribution from the Pacific Ocean in southern sites (COL and IRR, Fig. 4). Interannual PC1 $\delta^{18}O$ variability, as well as the differences in $\delta^{18}O$ across the *P. tarapacana* gradient, can be useful to assess past monsoon activity. This relationship is physically linked by the Bolivian High (BH) activity, an upper-level high-pressure cell that develops over the Central Andes in response to the latent heat released by the summer's deep convection over the Amazon Basin (Lenters and Cook, 1997). Wet periods in the Altiplano are related to a pronounced southward displacement of the BH, which allows for the expansion of the upper-air easterly flow and the ingress over the Altiplano of the moisture influx from the Amazon Basin (Lenters and Cook, 1997). It is interesting that as we move southward along our gradient of $\delta^{18}O$ *P. tarapacana* sites, the relationships between the $\delta^{18}O$ *P. tarapacana* chronologies and the $\delta^{18}O$ *C. odorata* record in the Bolivian Amazon decreases (Fig. S4). This also confirms the HYSPLIT results of a decreasing number of tropical air parcels arriving toward our southern *P. tarapacana* sites.

The climate of the *P. tarapacana* woodlands in the southern Tropical Andes is characterized by a high concentration of precipitation (>80% annual total) and warmer temperatures during the summer (Fig. 1c). Consequently, an increase in relative humidity and VPD occurs when the South American summer monsoon becomes more intense during summer (Fig. S5; Vera et al., 2006). Under this climatic context, the changes of $\delta^{18}O$ in *P. tarapacana* tree-ring cellulose in response to the environmental variability considered in this study (precipitation, mean temperature, soil moisture 0–10 cm and 10–40 cm, OLR, VPD, and wind circulation) are consistent. Firstly, variables related to moisture showed

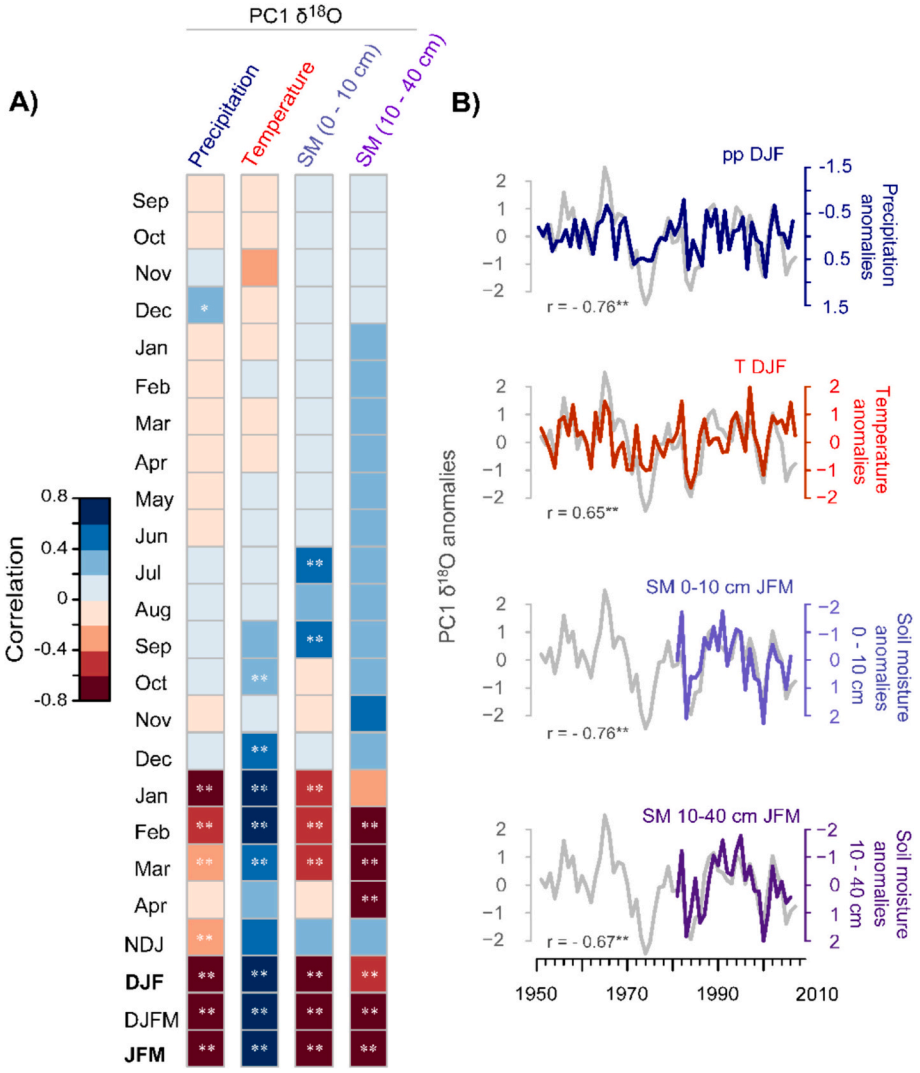

Fig. 5. Relationships between the time series of PC1 from the six δ18O *Polylepis tarapacana* chronologies (PC1 δ18O) and regional series of precipitation (pp) and temperature (T) (period 1956–2007), and regionally averaged soil moisture (SM) (0–10 cm and 10–40 cm depth) based on FLDAS (Land Data Assimilation System; period 1988–2007). (a) Correlation functions between PC1 δ18O and pp., T and SM presented for 20 months, from the prior (September) to the current year of ring formation (April), and for different combinations of summer months (NDJ: November, December, and January, DJF: December, January and February, DJFM: December, January, February and March, JFM: January, February and March. Asterisks denotes significant correlations at $*p < 0.05$ and $**p < 0.01$. (b) Comparisons between the normalized anomalies of PC1 δ18O *P. tarapacana* and pp., T and SM (0–10 cm and 10–40 cm depth) during the summer. All correlations were performed over prewhitened (AR(0)) time series. Note that the Y axes of the precipitation, soil moisture (0–10 cm) and soil moisture (10–40 cm) series (in B) are inverted to facilitate visual comparison.

a negative relationship with PC1 $\delta^{18}O$ (Fig. 5), which is consistent with lower $\delta^{18}O$ values when precipitation increases (Risi et al., 2008). This occurs because as relative humidity increases, water demand from the leaf decreases, and consequently, the evaporative enrichment of water from the leaf is reduced. The stomata remain open, and there is no $\delta^{18}O$ enrichment (Roden et al., 2000). In the case of soil moisture, the $\delta^{18}O$ values observed in tree rings are likely influenced by soil water evaporation, leading to an increase in the isotopic composition of the water absorbed by trees (Bailey et al., 2023). Secondly, mean temperature and VPD exhibited positive relationships with PC1 $\delta^{18}O$ (Figs. 5, 6b, 7b). This is consistent with an enrichment of $\delta^{18}O$ when temperature and VPD increase, resulting in the evaporation of water from the leaf and thus a lighter ^{16}O isotope (Roden et al., 2000). Another important point is the significant relationships between PC1 $\delta^{18}O$ and climate primarily registered during the current growing season. This may indicate that sugars utilized for the synthesis of cellulose are synthesized and fixed in the wood during the current growing season (Rathgeber et al., 2016; Rodríguez-Catón et al., 2021).

The main mode of $\delta^{18}O$ from the *P. tarapacana* network indicates significant positive relations with OLR and VDP during the summer (Fig. 7). This suggests that higher values of OLR and VPD –therefore, lower convection, less cloudiness, drier environmental conditions, and higher evapotranspiration– would lead to a $\delta^{18}O$ *P. tarapacana* tree-ring enrichment. This positive relationship between VPD and $\delta^{18}O$ encompasses a subcontinental region across the Tropical Andes and the Amazon basin (Fig. 7b). Our study suggests that VPD should be considered an important factor to gain insights into the tropical hydrologic cycle in this region of South America. An increase in VPD across the Amazon basin has been recently reported for the period 1979–2015 (Barkhordarian et al., 2019), implying a concomitant reduction in photosynthesis and vegetation growth since the 1990s (Yuan et al., 2019). This is particularly relevant considering the projected increase in aridity in the southern Tropical Andes for the 21st century (Minvielle and Garreaud, 2011; Neukom et al., 2015; Salazar et al., 2023), and the global projected increase in VPD (Yuan et al., 2019).

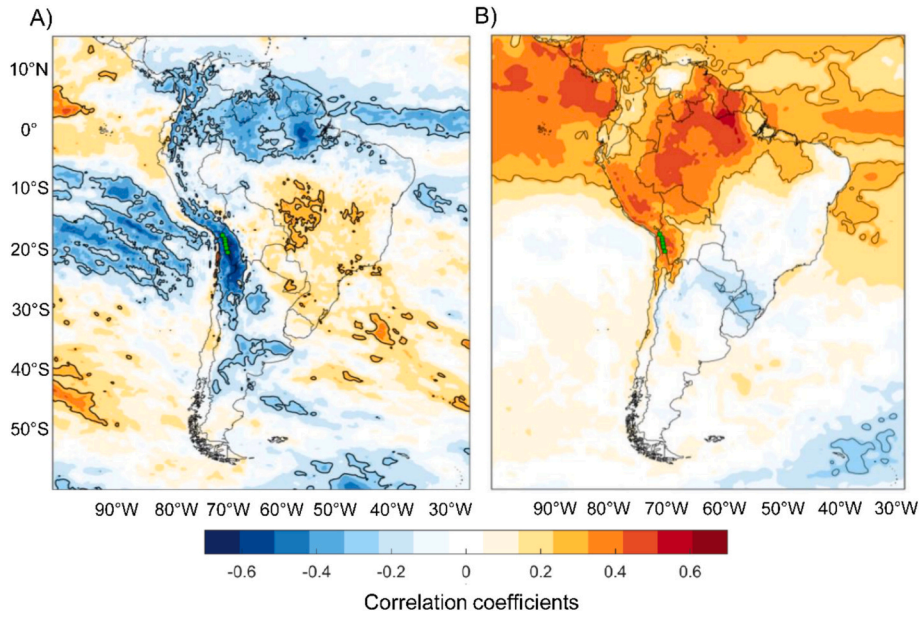

Fig. 6. Correlation map between the PC1 from the six $\delta^{18}O$ *Polylepis tarapacana* chronologies (PC1 $\delta^{18}O$) and gridded ERA5 fields of (a) precipitation and (b) temperature. Both correlation maps were calculated using summer (DJFM) gridded data of the current growing season and covering the period 1950–2007. Significant correlation values ($p < 0.05$) are demarcated in both maps by the continuous black lines and the green squares indicate the location of the $\delta^{18}O$ chronologies of *P. tarapacana*. All correlations were performed over prewhitened (AR(0)) time series. (For interpretation of the references to colour in this figure legend, the reader is referred to the web version of this article.)

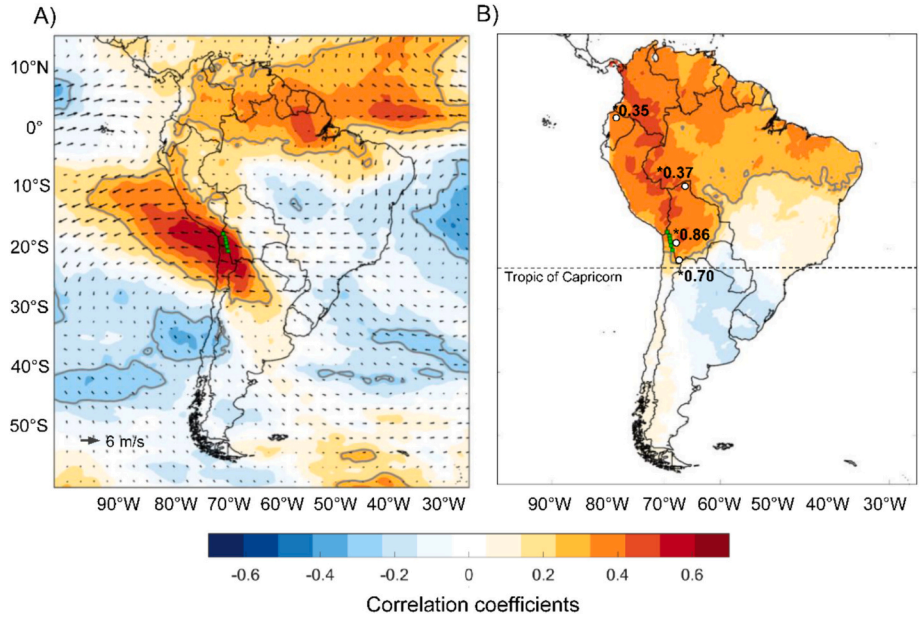

Fig. 7. Relationships between the PC1 from the six $\delta^{18}O$ *Polylepis tarapacana* chronologies (PC1 $\delta^{18}O$) and hydroclimate-related features over South America. (a) Correlation map between the PC1 and Outgoing Longwave Radiation (OLR) gridded data for the summer season (DJFM) during the current growing season (period 1950–2007), and on the top of that a composite map of summer (DJFM) mean 200 hPa zonal and meridional wind components depicted by the black vectors from the difference between the 10 wettest and the 10 driest years indicated by the PC1 $\delta^{18}O$ time series during the 1950–2008 period. OLR and wind gridded data (0.25° x 0.25°) obtained from ERA5. (b) Correlation map between the PC1 $\delta^{18}O$ time series and mean VPD summer (DJFM) gridded data (0.5° x 0.5°; derived from CRU) during the period 1950–2007. Notel that the correlation signal with VPD extends across the entire Tropical Andes region. The numbers indicate the correlation between the PC1 $\delta^{18}O$ and the $\delta^{18}O$ chronologies of *Cedrela montana* and *Cedrela odorata* from Baker et al. (2015, 2022) located in in the Ecuadorian Andes (>2000 km away) and the tropical lowlands of northern Bolivia (~1000 km away), respectively, and with the $\delta^{18}O$ *P. tarapacana* chronologies from Rodríguez-Catón et al. (2021) in the southern tropical Bolivian Andes (period 1950–2007; *$p < 0.01$). Significant correlation grids ($p < 0.05$) are depicted in both maps (a and b) by continuous grey lines, and the green squares indicate the location of the six $\delta^{18}O$ *P. tarapacana* chronologies. All correlations were performed over prewhitened (AR(0)) time series. Note that the wind composite map in (a) were calculated as the difference between the composite maps of the 10 highest and 10 lowest PC1 $\delta^{18}O$ values (years) as indicators of the 10 driest and 10 wettest years, respectively. (For interpretation of the references to colour in this figure legend, the reader is referred to the web version of this article.)

4.3. Implications for assessing long-term regional hydroclimate

Our results show that hydroclimate variability strongly controls $\delta^{18}O$ *P. tarapacana* content across our network, and that large-scale atmospheric circulation signals across the Tropical Andes and the Amazon basin are registered in the developed tree-ring network. This is consistent with other $\delta^{18}O$ tree-ring records from the Tropical Andes (Baker et al., 2015, 2022; Rodríguez-Catón et al., 2021, 2024; Vargas et al., 2022), and $\delta^{18}O$ signal in tropical Andean ice cores (Vuille et al., 2003). Moreover, our new network of $\delta^{18}O$ chronologies has proven to be useful for understanding the spatial variability of $\delta^{18}O$ in *P. tarapacana* tree-rings across the entire distribution of the species in the tropical Chilean Andes adjacent to the Atacama Desert. This study represents the first assessment of the relationships between a regional $\delta^{18}O$ signal contained in *P. tarapacana* tree-rings across its entire distribution in the western slopes of the southern Tropical Andes with environmental variables from local to subcontinental scales. The previous highlights the potential to develop future reconstructions of these parameters utilizing the main regional mode of $\delta^{18}O$ contained in *P. tarapacana* tree-rings, improving our current perspective based on individual sites and thus increasing the regional coverage of these registries to capture subcontinental signals throughout the Tropical Andes (Rodríguez-Catón et al., 2024). The development of this type of reconstructions will help us to better understand the variability of the tropical Andean hydroclimate. Moreover, the high common signal between the $\delta^{18}O$ variability from our tree-ring network, its relation with others $\delta^{18}O$ tree-ring chronologies in the Andean tropic, and the existing of $\delta^{18}O$ records of ice cores (Vimeux et al., 2009) and speleothems (Apaéstegui et al., 2018) in the Tropical Andes, open a new avenue to combine these paleoenvironmental records and improve our understanding of past climate variability and changes in Tropical South America.

CRediT authorship contribution statement

Claudio Álvarez: Writing – review & editing, Writing – original draft, Methodology, Formal analysis, Data curation, Conceptualization. **Duncan A. Christie:** Writing – review & editing, Supervision, Resources, Methodology, Formal analysis, Data curation, Conceptualization. **Álvaro González-Reyes:** Writing – review & editing, Supervision, Formal analysis, Conceptualization. **Thomas T. Veblen:** Writing – review & editing, Supervision. **Gerhard Helle:** Writing – review & editing, Supervision, Methodology, Formal analysis. **Carlos LeQuesne:** Writing – review & editing, Supervision. **Milagros Rodriguez-Caton:** Writing – review & editing. **Paul Szejner:** Writing – review & editing. **Felipe Flores:** Writing – review & editing, Methodology. **Tania Gipoulou-Zúñiga:** Writing – review & editing. **Manuel Suazo-Álvarez:** Writing – review & editing, Formal analysis. **Tomás Muñoz-Salazar:** Writing – review & editing. **Diego Aliste:** Writing – review & editing, Methodology. **Mariano S. Morales:** Writing – review & editing. **Ariel Muñoz:** Writing – review & editing. **Ricardo Villalba:** Writing – review & editing.

Declaration of competing interest

The authors declare that they have no known competing financial interests or personal relationships that could have appeared to influence the work reported in this paper.

Data availability

Data will be made available on request.

Acknowledgments

This research was funded by the Chilean Research Council (ANID) grants: FONDECYT 1241699, FONDAP/1523A0002, ANID/BASALFB210018, and REDES 180187 Chile-Germany. We acknowledge the Chilean Forest Service CONAF for permission to collect tree-ring samples in Las Vicuñas and Salar de Surire national Protected Areas. C.A. thanks for financial support from ANID PFCHA/Doctorado Nacional/2018-21181009 and postdoctoral fellowship from the Cape Horn International Center (CHIC). M. S-A. thanks for financial support from ANID Magister Nacional/ 2024-22240202 and graduate fellowship from the Cape Horn International Center (CHIC). T. M-S. thanks ANID-Subdirección de Capital Humano/Doctorado Nacional /2021–21210653. We thank two anonymous referees for their helpful comments on the manuscript.

Appendix A. Supplementary data

Supplementary data to this article can be found online at https://doi.org/10.1016/j.gloplacha.2024.104503.

References

Akaike, H., 1974. A new look at the statistical model identification. IEEE Trans. Autom. Control 19, 716–723. https://doi.org/10.1109/tac.1974.1100705.

Ancapichún, S., De Pol-Holz, R., Christie, D.A., Santos, G.M., Collado-Fabbri, S., Garreaud, R., Lambert, F., Orfanoz-Cheuquelaf, A., Rojas, M., Southon, J., Turnbull, J.C., Creasman, P.P., 2021. Radiocarbon bomb-peak signal in tree-rings from the tropical Andes register low latitude atmospheric dynamics in the Southern Hemisphere. Sci. Total Environ. 774, 145126 https://doi.org/10.1016/j.scitotenv.2021.145126.

Anderson, T.G., Christie, D.A., Chávez, R.O., Olea, M., Anchukaitis, K.J., 2021. Spatiotemporal peatland productivity and climate relationships across the western South American Altiplano. J. Geophys. Res. Biogeosci. 126 https://doi.org/10.1029/2020jg005994.

Apaéstegui, J., Cruz, F.W., Vuille, M., Fohlmeister, J., Espinoza, J.C., Sifeddine, A., Strikis, N., Guyot, J.L., Ventura, R., Cheng, H., Edwards, R.L., 2018. Precipitation changes over the eastern Bolivian Andes inferred from speleothem ($\delta^{18}O$) records for the last 1400 years. Earth Planet. Sci. Lett. 494, 124–134. https://doi.org/10.1016/j.epsl.2018.04.048.

Bailey, K., Szejner, P., Strange, B., Monson, R.K., Hu, J., 2023. The influence of winter snowpack on the use of summer rains in Montane pine forests across the southwest U.S. J. Geophys. Res. Biogeosci. 128 https://doi.org/10.1029/2023jg007494.

Baker, J.C.A., Hunt, S.F.P., Clerici, S.J., Newton, R.J., Bottrell, S.H., Leng, M.J., Heaton, T.H.E., Helle, G., Argollo, J., Gloor, M., Brienen, R.J.W., 2015. Oxygen isotopes in tree rings show good coherence between species and sites in Bolivia. Glob. Planet. Chang. 133, 298–308. https://doi.org/10.1016/j.gloplacha.2015.09.008.

Baker, J.C.A., Cintra, B.B.L., Gloor, M., Boom, A., Neill, D., Clerici, S., Leng, M.J., Helle, G., Brienen, R.J.W., 2022. The changing Amazon hydrological cycle—inferences from over 200 years of tree-ring oxygen isotope data. J. Geophys. Res. Biogeosci. 127 https://doi.org/10.1029/2022jg006955.

Barbour, M.M., Roden, J.S., Farquhar, G.D., Ehleringer, J.R., 2004. Expressing leaf water and cellulose oxygen isotope ratios as enrichment above source water reveals evidence of a Péclet effect. Oecologia 138, 426–435. https://doi.org/10.1007/s00442-003-1449-3.

Barkhordarian, A., Saatchi, S.S., Behrangi, A., Loikith, P.C., Mechoso, C.R., 2019. A recent systematic increase in vapor pressure deficit over tropical South America. Sci. Rep. 9, 15331. https://doi.org/10.1038/s41598-019-51857-8.

Blasing, T.J., Solomon, A.M., Duvick, D.N., 1984. Response functions revisited. Tree-Ring Bull. 44, 1–15.

Boisier, P., 2023. CR2MET: A High-Resolution Precipitation and Temperature Dataset for the Period 1960-2021 in Continental Chile. (v2.5) [Data Set]. Zenodo. https://doi.org/10.5281/zenodo.7529682.

Braun, G., 1997. The use of digital methods in assessing forest patterns in an Andean environment: the *Polylepis* example. Mt. Res. Dev. 17, 253–262. https://doi.org/10.2307/3673852.

Brienen, R.J.W., Helle, G., Pons, T.L., Guyot, J.-L., Gloor, M., 2012. Oxygen isotopes in tree rings are a good proxy for Amazon precipitation and El Niño-Southern oscillation variability. Proc. Natl. Acad. Sci. USA 109, 16957–16962. https://doi.org/10.1073/pnas.1205977109.

Briffa, K.R., 1995. Interpreting high-resolution proxy climate data — the example of dendroclimatology. In: Analysis of Climate Variability. Springer Berlin Heidelberg, Berlin, Heidelberg, pp. 77–94.

Bunn, A.G., 2008. A dendrochronology program library in R (dplR). Dendrochronologia (Verona) 26, 115–124. https://doi.org/10.1016/j.dendro.2008.01.002.

Canedo-Rosso, C., Hochrainer-Stigler, S., Pflug, G., Condori, B., Berndtsson, R., 2021. Drought impact in the Bolivian Altiplano agriculture associated with the El Niño–Southern oscillation using satellite imagery data. Nat. Hazards Earth Syst. Sci. 21, 995–1010. https://doi.org/10.5194/nhess-21-995-2021.

Carslaw, D.C., Ropkins, K., 2012. Openair — an R package for air quality data analysis. Environ. Model Softw. 27–28, 52–61. https://doi.org/10.1016/j.envsoft.2011.09.008.

Christie, D.A., Lara, A., Barichivich, J., Villalba, R., Morales, M.S., Cuq, E., 2009. El Niño-Southern oscillation signal in the world's highest-elevation tree-ring chronologies from the Altiplano, Central Andes. Palaeogeogr. Palaeoclimatol. Palaeoecol. 281, 309–319. https://doi.org/10.1016/j.palaeo.2007.11.013.

Christie, D.A., Boninsegna, J.A., Cleaveland, M.K., Lara, A., Le Quesne, C., Morales, M.S., Mudelsee, M., Stahle, D.W., Villalba, R., 2011. Aridity changes in the temperate-mediterranean transition of the Andes since ad 1346 reconstructed from tree-rings. Clim. Dyn. 36, 1505–1521. https://doi.org/10.1007/s00382-009-0723-4.

Cook, E.R., Pederson, N., 2011. Uncertainty, emergence, and statistics in dendrochronology. In: Dendroclimatology. Springer Netherlands, Dordrecht, pp. 77–112.

Cook, E.R., Briffa, K., Shiyatov, S., Mazepa, V., 1990. Tree ring standardization and growth-trend estimation. In: Cook, E., Kairiuktis, L. (Eds.), Methods of Dendro-Chronology. Kluwer Academic Publishers, Dordrecht, pp. 104–132.

Craig, H., Gordon, L.I., 1965. Deuterium and oxygen 18 variations in the ocean and the marine atmosphere. In: Tongiogi, E., Lishi, E., V. (Eds.), Proc. Stable Isotopes in Oceanographic Studies and Paleotemperatures, Spoleto, Italy, pp. 9–130.

Cuyckens, G.A.E., Christie, D.A., Domic, A.I., Malizia, L.R., Renison, D., 2016. Climate change and the distribution and conservation of the world's highest elevation woodlands in the South American Altiplano. Glob. Planet. Chang. 137, 79–87. https://doi.org/10.1016/j.gloplacha.2015.12.010.

Dansgaard, W., 1964. Stable isotopes in precipitation. Tellus 16, 436–468. https://doi.org/10.1111/j.2153-3490.1964.tb00181.x.

Dawdy, D.R., Matalas, N.C., 1964. Statistical and probability analysis of hydrologic data. Part III. Analysis of variance, covariance, and time series. In: Chow, V.T. (Ed.), Handbook of Applied Hydrology: A Compendium of Water-Resources Technology. McGraw-Hill, New York, pp. 868–890.

Dee, D.P., Uppala, S., Simmons, A., Berrisford, P., Poli, P., Kobayashi, S., Andrae, U., Balmaseda, M.A., Balsamo, G., Bauer, P., Bechtold, P., Beljaars, A.C.M., van de Berg, L., Bidlot, J., Bormann, N., Delsol, C., Dragani, R., Fuentes, M., Geer, A.J., Haimberger, L., Healy, S.B., Hersbach, H., Hólm, E.V., Isaksen, L., Kållberg, P., Köhler, M., Matricardi, M., McNally, A.P., Monge-Sanz, B.M., Morcrette, J.J., Park, B.K., Peubey, C., de Rosnay, P., Tavolato, C., Thépaut, J.N., Vitart, F., 2011. The ERA-Interim reanalysis: configuration and performance of the data assimilation system. Q. J. R. Meteorol. Soc. 137 (656), 553–597. https://doi.org/10.1002/qj.828.

Draxler, R., Hess, G., 1998. An overview of the HYSPLIT_4modeling system for trajectories, dispersion, and deposition. Aust. Meteorol. Mag. 47, 295–308.

Draxler, R.R., Taylor, A.D., 1982. Horizontal dispersion parameters for long-range transport modeling. J. Appl. Meteorol. 21, 367–372. https://doi.org/10.1175/1520-0450(1982)021<0367:hdpflr>2.0.co;2.

Falvey, M., Garreaud, R.D., 2005. Moisture variability over the South American Altiplano during the South American low level jet experiment (SALLJEX) observing season. J. Geophys. Res. 110 https://doi.org/10.1029/2005jd006152.

Farquhar, G., Lloyd, J., 1993. Carbon and oxygen isotope effects in the exchange of carbon dioxide between terrestrial plants and the atmosphere. In: Ehleringer, J.R., Hall, A.E., Farquhar, G.D. (Eds.), Stable Isotopes and Carbon-Water Relations. Academic Press.

Freund, M.B., Helle, G., Balting, D.F., Ballis, N., Schleser, G.H., Cubasch, U., 2023. European tree-ring isotopes indicate unusual recent hydroclimate. Commun. Earth Environ. 4 https://doi.org/10.1038/s43247-022-00648-7.

Fritts, H.C., 1976. Tree Rings and Climate. Academic Press, London, p. 567.

Gagen, M., Carroll, D., Loader, N., Robertson, I., 2010. Stables isotopes in dendroclimatology: moving beyond potential. In: Hughes, M.K., Swetnam, T.W., Diaz, H.F. (Eds.), Dendroclimatology: Progress and Prospects. Developments in Paleoenvironmental Research.

García-Plazaola, J.I., Rojas, R., Christie, D.A., Coopman, R.E., 2015. Photosynthetic responses of trees in high-elevation forests: comparing evergreen species along an elevation gradient in the Central Andes. AoB Plants 7, lv058. https://doi.org/10.1093/aobpla/plv058.

Garreaud, R., 1999. A multi-scale analysis of the summertime precipitation over the Central Andes. Mon. Weather Rev. 127, 901–921.

Garreaud, R., Aceituno, P., 2001. Interannual rainfall variability over the South American Altiplano. J. Clim. 14, 2779–2789. https://doi.org/10.1175/1520-0442(2001)014<2779:irvots>2.0.co;2.

Garreaud, R., Vuille, M., Clement, A.C., 2003. The climate of the Altiplano: observed current conditions and mechanisms of past changes. Palaeogeogr. Palaeoclimatol. Palaeoecol. 194, 5–22. https://doi.org/10.1016/s0031-0182(03)00269-4.

Harris, I., Osborn, T.J., Jones, P., Lister, D., 2020. Version 4 of the CRU TS monthly high-resolution gridded multivariate climate dataset. Sci. Data 7, 109. https://doi.org/10.1038/s41597-020-0453-3.

Hartmann, D.L., 2016. Global Physical Climatology, Second edition. Elsevier. https://doi.org/10.1016/C2009-0-00030-0.

Helle, G., et al., 2022. Stable isotope signatures of wood, its constituents and methods of cellulose extraction. In: Siegwolf, R.T.W., Brooks, J.R., Roden, J., Saurer, M. (Eds.), Stable Isotopes in Tree Rings: Inferring Physiological, Climatic and Environmental Responses. Springer International Publishing, Cham, pp. 135–190.

Hersbach, H., Bell, B., Berrisford, P., Hirahara, S., Horányi, A., Muñoz-Sabater, J., Nicolas, J., Peubey, C., Radu, R., Schepers, D., Simmons, A., Soci, C., Abdalla, S., Abellan, X., Balsamo, G., Bechtold, P., Biavati, G., Bidlot, J., Bonavita, M., Chiara, G., Dahlgren, P., Dee, D., Diamantakis, M., Dragani, R., Flemming, J., Forbes, R., Fuentes, M., Geer, A., Haimberger, L., Healy, S., Hogan, R.J., Hólm, E., Janisková, M., Keeley, S., Laloyaux, P., Lopez, P., Lupu, C., Radnoti, G., Rosnay, P., Rozum, I., Vamborg, F., Villaume, S., Thépaut, Jean-Noël, 2020. The ERA5 global reanalysis. Q. J. R. Meteorol. Soc. 146, 1999–2049. https://doi.org/10.1002/qj.3803.

Holmes, R.L., 1983. Computer-assisted quality control in tree-ring dating and measurement. Tree-Ring Bull. 43, 69–78.

Hsieh, J.C.C., Chadwick, O.A., Kelly, E.F., Savin, S.M., 1998. Oxygen isotopic composition of soil water: quantifying evaporation and transpiration. Geoderma 82, 269–293. https://doi.org/10.1016/s0016-7061(97)00105-5.

Kalnay, E., Kanamitsu, M., Kistler, R., Collins, W., Deaven, D., Gandin, L., Iredell, M., Saha, S., White, G., Woollen, J., Zhu, Y., Leetmaa, A., Reynolds, R., Chelliah, M., Ebisuzaki, W., Higgins, W., Janowiak, J., Mo, K.C., Ropelewski, C., Wang, J., Jenne, R., Joseph, D., 1996. The NCEP/NCAR 40-year reanalysis project. Bull. Am. Meteorol. Soc. 77, 437–471. https://doi.org/10.1175/1520-0477(1996)077<0437:tnyrp>2.0.co;2.

Laumer, W., et al., 2009. A novel approach for the homogenization of cellulose to use micro-amounts for stable isotope analyses. Rapid Commun. Mass Spectrom. 23 (13), 1934–1940.

Leavitt, S.W., Lone, A., 1991. Seasonal stable-carbon isotope variability in tree rings: possible paleoenvironmental signals. Chem. Geol. 87, 59–70. https://doi.org/10.1016/0168-9622(91)90033-s.

Lenters, J.D., Cook, K.H., 1997. On the origin of the Bolivian high and related circulation features of the South American climate. J. Atmos. Sci. 54, 656–678. https://doi.org/10.1175/1520-0469(1997)054<0656:otootb>2.0.co;2.

Liebmann, B., Smith, C.A., 1996. Description of a Complete (Interpolated) Outgoing.

Martens, B., Miralles, D.G., Lievens, H., van der Schalie, R., de Jeu, R.A.M., Fernández-Prieto, D., Beck, H.E., Dorigo, W.A., Verhoest, N.E.C., 2017. GLEAM v3: satellite-based land evaporation and root-zone soil moisture. Geosci. Model Dev. 10, 1903–1925. https://doi.org/10.5194/gmd-10-1903-2017.

McNally, A., Arsenault, K., Kumar, S., Shukla, S., Peterson, P., Wang, S., Funk, C., Peters-Lidard, C.D., Verdin, J.P., 2017. A land data assimilation system for sub-Saharan Africa food and water security applications. Sci. Data 4 (1). https://doi.org/10.1038/sdata.2017.12.

Meier, W.J.-H., Aravena, J.-C., Jaña, R., Braun, M.H., Hochreuther, P., Soto-Rogel, P., Grießinger, J., 2020. A tree-ring δ18O series from southernmost Fuego-Patagonia is recording flavors of the Antarctic Oscillation. Glob. Planet. Change 195, 103302. https://doi.org/10.1016/j.gloplacha.2020.103302.

Messerli, B., Grosjean, M., Vuille, M., 1997. Water availability, protected areas, and natural resources in the Andean desert Altiplano. Mt. Res. Dev. 17, 229–238. https://doi.org/10.2307/3673850.

Minvielle, M., Garreaud, R.D., 2011. Projecting rainfall changes over the South American Altiplano. J. Clim. 24, 4577–4583. https://doi.org/10.1175/jcli-d-11-00051.1.

Morales, M.S., Christie, D.A., Villalba, R., Argollo, J., Pacajes, J., Silva, J.S., Alvarez, C. A., Llancabure, J.C., Solíz Gamboa, C.C., 2012. Precipitation changes in the South American Altiplano since 1300 AD reconstructed by tree-rings. Clim. Past 8, 653–666. https://doi.org/10.5194/cp-8-653-2012.

Morales, M.S., Cook, E.R., Barichivich, J., Christie, D.A., Villalba, R., LeQuesne, C., Srur, A.M., Ferrero, M.E., González-Reyes, Á., Couvreux, F., Matskovsky, V., Aravena, J.C., Lara, A., Mundo, I.A., Rojas, F., Prieto, M.R., Smerdon, J.E., Bianchi, L.O., Masiokas, M.H., Urrutia-Jalabert, R., Rodríguez-Catón, M., Muñoz, A. A., Rojas-Badilla, M., Alvarez, C., Lopez, L., Luckman, B.H., Lister, D., Harris, I., Jones, P.D., Williams, A.P., Velazquez, G., Aliste, D., Aguilera-Betti, I., Marcotti, E., Flores, F., Muñoz, T., Cuq, E., Boninsegna, J.A., 2020. Six hundred years of South American tree rings reveal an increase in severe hydroclimatic events since mid-20th century. Proc. Natl. Acad. Sci. USA 117, 16816–16823. https://doi.org/10.1073/pnas.2002411117.

Morales, M.S., Crispín-DelaCruz, D.B., Álvarez, C., Christie, D.A., Ferrero, M.E., Andreu-Hayles, L., Villalba, R., Guerra, A., Ticse-Otarola, G., Rodríguez-Ramírez, E.C., LLoccla-Martínez, R., Sanchez-Ferrer, J., Requena-Rojas, E.J., 2023. Drought increase since the mid-20th century in the northern South American Altiplano revealed by a 389-year precipitation record. Clim. Past 19, 457–476. https://doi.org/10.5194/cp-19-457-2023.

Nagavciuc, V., Ionita, M., Kern, Z., McCarroll, D., Popa, I., 2022. A ~700 years perspective on the 21st century drying in the eastern part of Europe based on δ18O in tree ring cellulose. Commun. Earth Environ. 3 https://doi.org/10.1038/s43247-022-00605-4.

Nagavciuc, V., Michel, S.L.L., Balting, D.F., Helle, G., Freund, M., Schleser, G.H., Steger, D.N., Lohmann, G., Ionita, M., 2024. A past and present perspective on the European summer vapor pressure deficit. Clim. Past 20, 573–595. https://doi.org/10.5194/cp-20-573-2024.

Naulier, M., Savard, M.M., Bégin, C., Gennaretti, F., Arseneault, D., Marion, J., Nicault, A., Bégin, Y., 2015. A millennial summer temperature reconstruction for northeastern Canada using oxygen isotopes in subfossil trees. Clim. Past 11, 1153–1164. https://doi.org/10.5194/cp-11-1153-2015.

Neukom, R., Rohrer, M., Calanca, P., Salzmann, N., Huggel, C., Acuña, D., Christie, D.A., Morales, M.S., 2015. Facing unprecedented drying of the Central Andes? Precipitation variability over the period AD 1000–2100. Environ. Res. Lett. 10, 084017 https://doi.org/10.1088/1748-9326/10/8/084017.

Paul, D., Skrzypek, G., Forizs, I., 2007. Normalization of measured stable isotopic compositions to isotope reference scales–a review. Rapid Commun. Mass Spectrom. 21 (18), 3006–3014.

Pawlowicz, R., 2020. M_Map: A Mapping Package for MATLAB. version 1.4m, [Computer software], available online at. www.eoas.ubc.ca/~rich/map.html.

R Development Core Team, 2021. R: A Language and Environment for Statistical Computing. R Foundation for Statistical Computing, Vienna, Austria. URL. https://www.R-project.org/.

Rathgeber, C.B.K., Cuny, H.E., Fonti, P., 2016. Biological basis of tree-ring formation: a crash course. Front. Plant Sci. 7, 734. https://doi.org/10.3389/fpls.2016.00734.

Rawson, H.M., Begg, J.E., Woodward, R.G., 1977. The effect of atmospheric humidity on photosynthesis, transpiration and water use efficiency of leaves of several plant species. Planta 134, 5–10. https://doi.org/10.1007/BF00390086.

Rinne, K.T., Loader, N.J., Switsur, V.R., Waterhouse, J.S., 2013. 400-year May–August precipitation reconstruction for Southern England using oxygen isotopes in tree rings. Quat. Sci. Rev. 60, 13–25. https://doi.org/10.1016/j.quascirev.2012.10.048.

Risi, C., Bony, S., Vimeux, F., 2008. Influence of convective processes on the isotopic composition ($\delta^{18}O$ and δD) of precipitation and water vapor in the tropics: 2. Physical interpretation of the amount effect. J. Geophys. Res. 113 https://doi.org/10.1029/2008jd009943.

Roden, J.S., Lin, G., Ehleringer, J.R., 2000. A mechanistic model for interpretation of hydrogen and oxygen isotope ratios in tree-ring cellulose. Geochim. Cosmochim. Acta 64, 21–35. https://doi.org/10.1016/s0016-7037(99)00195-7.

Rodríguez-Catón, M., Andreu-Hayles, L., Morales, M.S., Daux, V., Christie, D.A., Coopman, R.E., Alvarez, C., Rao, M.P., Aliste, D., Flores, F., Villalba, R., 2021. Different climate sensitivity for radial growth, but uniform for tree-ring stable isotopes along an aridity gradient in *Polylepis tarapacana*, the world's highest elevation tree species. Tree Physiol. 41, 1353–1371. https://doi.org/10.1093/treephys/tpab021.

Rodríguez-Catón, M., Andreu-Hayles, L., Daux, V., Vuille, M., Varuolo-Clarke, A.M., Oelkers, R., Christie, D.A., D'Arrigo, R., Morales, M.S., Palat Rao, M., Srur, A.M., Vimeux, F., Villalba, R., 2022. Hydroclimate and ENSO variability recorded by oxygen isotopes from tree rings in the South American Altiplano. Geophys. Res. Lett. 49 https://doi.org/10.1029/2021gl095883.

Rodríguez-Catón, M., Morales, M.S., Rao, M.P., Nixon, T., Vuille, M., Rivera, J.A., Oelkers, R., Christie, D.A., Varuolo-Clarke, A.M., Ferrero, M.E., Magney, T., Daux, V., Villalba, R., Andreu-Hayles, L., 2024. A 300-year tree-ring δ18O-based precipitation reconstruction for the South American Altiplano highlights decadal hydroclimate teleconnections. Commun. Earth Environ. https://doi.org/10.1038/s43247-024-01385-9.

Salazar, A., Thatcher, M., Goubanova, K., Bernal, K., Gutiérrez, J., Squeo, F., 2023. CMIP6 precipitation and temperature projections for Chile. Clim. Dyn. https://doi.org/10.1007/s00382-023-07034-9.

Schulman, E., 1956. Dendroclimatic Change in Semiarid America. University of Arizona Press Tucson.

Solíz, C., Villalba, R., Argollo, J., Morales, M.S., Christie, D.A., Moya, J., Pacajes, J., 2009. Spatio-temporal variations in *Polylepis tarapacana* radial growth across the Bolivian Altiplano during the 20th century. Palaeogeogr. Palaeoclimatol. Palaeoecol. 281, 296–308. https://doi.org/10.1016/j.palaeo.2008.07.025.

Stein, A.F., Draxler, R.R., Rolph, G.D., Stunder, B.J.B., Cohen, M.D., Ngan, F., 2015. NOAA's HYSPLIT atmospheric transport and dispersion modeling system. Bull. Am. Meteorol. Soc. 96, 2059–2077. https://doi.org/10.1175/bams-d-14-00110.1.

Stokes, M.A., Smiley, T.L., 1968. An Introduction to Tree-Ring Dating. University of Chicago Press, Chicago, Ill.

Szejner, P., Clute, T., Anderson, E., Evans, M.N., Hu, J., 2020. Reduction in lumen area is associated with the $\delta^{18}O$ exchange between sugars and source water during cellulose synthesis. New Phytol. 226, 1583–1593. https://doi.org/10.1111/nph.16484.

Treydte, K., Boda, S., Graf Pannatier, E., Fonti, P., Frank, D., Ullrich, B., Saurer, M., Siegwolf, R., Battipaglia, G., Werner, W., Gessler, A., 2014. Seasonal transfer of oxygen isotopes from precipitation and soil to the tree ring: source water versus needle water enrichment. New Phytol. 202, 772–783. https://doi.org/10.1111/nph.12741.

Treydte, K., Liu, L., Padrón, R.S., Martínez-Sancho, E., Babst, F., Frank, D.C., Gessler, A., Kahmen, A., Poulter, B., Seneviratne, S.I., Stegehuis, A.I., Wilson, R., Andreu-Hayles, L., Bale, R., Bednarz, Z., Boettger, T., Berninger, F., Büntgen, U., Daux, V., Dorado-Liñán, I., Esper, J., Friedrich, M., Gagen, M., Grabner, M., Grudd, H., Gunnarsson, B.E., Gutiérrez, E., Hafner, P., Haupt, M., Hilasvuori, E., Heinrich, I., Helle, G., Jalkanen, R., Jungner, H., Kalela-Brundin, M., Kessler, A., Kirchhefer, A., Klesse, S., Krapiec, M., Levanič, T., Leuenberger, M., Linderholm, H.W., McCarroll, D., Masson-Delmotte, V., Pawelczyk, S., Pazdur, A., Planells, O., Pukiene, R., Rinne-Garmston, K.T., Robertson, I., Saracino, A., Saurer, M., Schleser, G.H., Seftigen, K., Siegwolf, R.T.W., Sonninen, E., Stievenard, M., Szychowska-Krapiec, E., Szymaszek, M., Todaro, L., Waterhouse, J.S., Weigl-Kuska, M., Weigt, R.B., Wimmer, R., Woodley, E.J., Vitas, A., Young, G., Loader, N. J., 2024. Recent human-induced atmospheric drying across Europe unprecedented in the last 400 years. Nat. Geosci. 17, 58–65. https://doi.org/10.1038/s41561-023-01335-8.

Vargas, D., Pucha-Cofrep, D., Serrano-Vincenti, S., Burneo, A., Carlosama, L., Herrera, M., Cerna, M., Molnár, M., Jull, A.J.T., Temovski, M., László, E., Futó, I., Horváth, A., Palcsu, L., 2022. ITCZ precipitation and cloud cover excursions control Cedrela nebulosa tree-ring oxygen and carbon isotopes in the northwestern Amazon. Glob. Planet. Chang. 211, 103791 https://doi.org/10.1016/j.gloplacha.2022.103791.

Vera, C., Higgins, W., Amador, J., Ambrizzi, T., Garreaud, R., Gochis, D., Gutzler, D., Lettenmaier, D., Marengo, J., Mechoso, C.R., Nogues-Paegle, J., Dias, P.L.S., Zhang, C., 2006. Toward a unified view of the American monsoon systems. J. Clim. 19, 4977–5000. https://doi.org/10.1175/jcli3896.1.

Vimeux, F., Ginot, P., Schwikowski, M., Vuille, M., Hoffmann, G., Thompson, L.G., Schotterer, U., 2009. Climate variability during the last 1000 years inferred from Andean ice cores: a review of methodology and recent results. Palaeogeogr. Palaeoclimatol. Palaeoecol. 281, 229–241. https://doi.org/10.1016/j.palaeo.2008.03.054.

Vuille, M., Keimig, F., 2004. Interannual variability of summertime convective cloudiness and precipitation in the Central Andes derived from ISCCP-B3 data. J. Clim. 17, 3334–3348. https://doi.org/10.1175/1520-0442(2004)017<3334:ivoscc>2.0.co;2.

Vuille, M., Bradley, R.S., Healy, R., Werner, M., Hardy, D.R., Thompson, L.G., Keimig, F., 2003. Modeling $\delta^{18}O$ in precipitation over the tropical Americas: 2. Simulation of the stable isotope signal in Andean ice cores. J. Geophys. Res. 108 (D6), 4175. https://doi.org/10.1029/2001JD002039.

Vuille, M., Franquist, E., Garreaud, R., Lavado Casimiro, W.S., Cáceres, B., 2015. Impact of the global warming hiatus on Andean temperature. J. Geophys. Res. 120, 3745–3757. https://doi.org/10.1002/2015jd023126.

Wigley, T.M.L., Briffa, K.R., Jones, P.D., 1984. On the average value of correlated time series, with applications in dendroclimatology and hydrometeorology. J. Clim. Appl. Meteorol. 23, 201–213. https://doi.org/10.1175/1520-0450(1984)023<0201:otavoc>2.0.co;2.

Xu, G., Liu, X., Sun, W., Szejner, P., Zeng, X., Yoshimura, K., Trouet, V., 2020. Seasonal divergence between soil water availability and atmospheric moisture recorded in intra-annual tree-ring $\delta^{18}O$ extremes. Environ. Res. Lett. 15, 094036 https://doi.org/10.1088/1748-9326/ab9792.

Yuan, W., Zheng, Y., Piao, S., Ciais, P., Lombardozzi, D., Wang, Y., Ryu, Y., Chen, G., Dong, W., Hu, Z., Jain, A.K., Jiang, C., Kato, E., Li, S., Lienert, S., Liu, S., Nabel, J.E. M.S., Qin, Z., Quine, T., Sitch, S., Smith, W.K., Wang, F., Wu, C., Xiao, Z., Yang, S., 2019. Increased atmospheric vapor pressure deficit reduces global vegetation growth. Sci. Adv. 5, eaax1396 https://doi.org/10.1126/sciadv.aax1396.

Zang, C., Biondi, F., 2015. Treeclim: an R package for the numerical calibration of proxy-climate relationships. Ecography 38, 431–436. https://doi.org/10.1111/ecog.01335.